



# Modeling heat exchangers with an open source DEM-based code for granular flows

Evan F. Johnson <sup>a, b</sup>, İlker Tari <sup>a</sup>, Derek Baker <sup>a</sup>

Show more

+ Add to Mendeley Share Cite

<https://doi.org/10.1016/j.solener.2021.09.067>

Get rights and content

How to Cite		BibTeX
<b>MLA</b>	Johnson, Evan F., İlker Tari, and Derek Baker. "Modeling heat exchangers with an open source DEM-based code for granular flows." <i>Solar Energy</i> 228 (2021): 374-386.	<pre>@article{johanson2021modeling,   title={Modeling heat exchangers with an open source DEM-based code for granular flows},   author={Johnson, Evan F and Tar{i}, {I.}lker and Baker, Derek},   journal={Solar Energy},   volume={228},   pages={374–386},   year={2021},   publisher={Elsevier} }</pre>
<b>APA</b>	Johnson, E. F., Tari, İ., & Baker, D. (2021). Modeling heat exchangers with an open source DEM-based code for granular flows. <i>Solar Energy</i> , 228, 374-386.	
<b>Chicago</b>	Johnson, Evan F., İlker Tari, and Derek Baker. "Modeling heat exchangers with an open source DEM-based code for granular flows." <i>Solar Energy</i> 228 (2021): 374-386.	
<b>Harvard</b>	Johnson, E.F., Tari, İ. And Baker, D., 2021. Modeling heat exchangers with an open source DEM-based code for granular flows. <i>Solar Energy</i> , 228, pp.374-386.	
<b>Vancouver</b>	Johnson EF, Tari İ, Baker D. Modeling heat exchangers with an open source DEM-based code for granular flows. <i>Solar Energy</i> . 2021 Nov 1;228:374-86.	
Links to Published Version <sup>1</sup>		
via Journal Website	<a href="https://www.sciencedirect.com/science/article/pii/S0038092X21008240">https://www.sciencedirect.com/science/article/pii/S0038092X21008240</a>	
via DOI	<a href="https://doi.org/10.1016/j.solener.2021.09.067">https://doi.org/10.1016/j.solener.2021.09.067</a>	
Links to Open Access (OA) Versions		
OA Pathway <sup>2</sup>	Embargo Period?	Link
Accepted Version <sup>3</sup> Pathway a	No	<a href="http://users.metu.edu.tr/dbaker/OpenAccess/doi.10.1016.j.solener.2021.09.067.pdf">http://users.metu.edu.tr/dbaker/OpenAccess/doi.10.1016.j.solener.2021.09.067.pdf</a>
Accepted Version <sup>3</sup> Pathway b	Yes	<a href="https://zenodo.org/record/5594171">https://zenodo.org/record/5594171</a>
Accepted Version <sup>3</sup> Pathway b	Yes	Provide a link to version deposited at OpenMETU.

This article was published OA using the *Smart OA Green+* route. *Guidelines to Support Smart OA* that include a description of the *Green+* OA route are published OA at <https://zenodo.org/record/5501401>.

#### Notes

<sup>1</sup> The Published Version, also referred to as the Version of Record (VoR), is the fully-formatted version of the article as published in the journal.

<sup>2</sup> The OA Pathway is defined using Sherpa Romeo (<https://v2.sherpa.ac.uk/romeo/>). The definitions for the relevant Pathways for this journal are attached after the manuscript as an appendix.

<sup>3</sup> The Accepted Version, also referred to as the Author Accepted Manuscript (AAM), is the accepted version of the manuscript submitted to the journal by the author. The Accepted Version does not include any typesetting or final proofing services provided by the journal to convert the Accepted Version into the Published Version. Thus, the Published Version and Accepted Version are identical in terms of scientific content, but differ in terms of formatting and final proofing.

# Modeling Heat Exchangers with an Open Source DEM-based Code for Granular Flows

Evan F. Johnson<sup>a,b,c</sup>, İlker Tari<sup>a</sup>, and Derek Baker<sup>a</sup>

<sup>a</sup>*Mechanical Engineering Department, Güneş Enerjisi Araştırma ve Uygulama Merkezi (ODTÜ-GÜNAM), Middle East Technical University, Üniversiteler Mahallesi, Dumlupınar Bulvarı*

*No:1, 06800 Çankaya Ankara, Turkey*

<sup>b</sup>*Present Address: Laboratory of Renewable Energy Science and Engineering, EPFL, Station 9, 1015, Lausanne, Switzerland*

<sup>c</sup>*evan.johnson@epfl.ch*

## Abstract

Dense granular flows exist in many solid particle heat exchangers and solar receivers studied in the field of Concentrating Solar Power (CSP). By tracking particles individually with the Discrete Element Method (DEM), the details of particle friction, collisions, and mixing can be modeled accurately. An open source DEM-based code for modeling heat transfer in dense granular flows is presented, called Dense Particle Heat Transfer (DPHT). It uses one-way coupling, with DEM run first to find the particle positions and DPHT run second to calculate heat transfer between particles and any walls. Heat transfer is computed with six sub-models, including effects from contact conduction, conduction through the thin fluid gap between particles, and thermal radiation. Simulations are run to investigate particle-particle radiation, with DPHT matching a full Monte Carlo ray tracing simulation to within 1.6%, whereas the “local environment temperature” models from literature show physically unrealistic results. As a test of the accuracy of DPHT, a simulation is run to replicate published experimental work, and results in terms of total heat transfer are within 4%. Finally, a tubular heat exchanger is analyzed, and a “radial” mixer design is introduced, increasing heat transfer by 8%. Several DEM-based heat transfer codes have been described in literature, but they are often kept in-house. Some open source codes exist as well, but they generally have drawbacks including missing heat transfer

modes, insufficient flexibility to make significant changes, and incomplete documentation. DPHT aims to simplify this modeling method by providing a flexible, open source solution.

*Keywords:* discrete element method; dense granular flow; particle heat exchanger; particle-scale heat transfer; solid particle solar receiver

## **1. Introduction**

Using solid particles to transfer and store heat is an important topic in Concentrating Solar Power (CSP) (Siegel et al., 2018)(Watkins, 2018), as well as in other processes such as limestone calcination for cement production (Komossa et al., 2015) and biomass pyrolysis (Qi and Wright, 2018). Detailed modeling of heat transfer in groups of flowing particles remains a challenge currently pursued by numerous researchers in these fields. The focus of this article is on dense granular flows, where the solid fraction is high (typically 0.52 to 0.64), and particle friction and collisions determine the behavior of the flow (Brennen, 2002). This is in contrast to fluidized or falling particles, which typically have a lower solid fraction. Dense granular flows can be found in many solar receivers and particle-fluid heat exchangers studied by CSP researchers (Albrecht and Ho, 2019)(Watkins, 2018)(Ruiz et al., 2019)(Niederwestberg et al., 2020)(Hicdurmaz et al., 2020)(Bartsch et al., 2016).

Modeling of particle flows can be separated broadly into continuum (Eulerian) approaches, where the bulk of particles is modeled as if it were a fluid, and Lagrangian approaches, where particles are modeled individually (Goniva et al., 2010). The leading Lagrangian method is the Discrete Element Method (DEM). Often, particles are surrounded by an “interstitial” fluid (such as air) which must be modeled as well, and together they comprise a two-phase system. Eulerian approaches model the two phases as intermixed fluids, and a modified version of the Navier-Stokes equations is solved, resulting in an “Euler-Euler” or “Two-Fluid” model. Alternatively, an “Euler-Lagrange” method can be employed for two-phase flow, where the fluid phase is modeled with Computational Fluid Dynamics (CFD), and particles are modeled with DEM, together forming a “coupled CFD-DEM” model.

Continuum models have been successfully employed in dilute flows such as fluidized beds (Hicdurmaz and Tari, 2018). However, in dense granular flows, the bulk flow does not behave as a fluid, as the motion is dictated by particle friction and collisions, which are determined by particle-scale phenomena such as friction coefficients, surface roughness, and hardness, which continuum models cannot easily replicate. In addition, unlike a fluid, particles pulled downward with gravity do not fill the gaps on the underside of any tubes or obstacles, leaving a cavity (Bartsch et al., 2016)(Brennen, 2002). This shows the need for DEM-based models in heat exchange devices with dense flows.

In DEM, each particle is modeled as a sphere, and when two spheres collide they are allowed to overlap slightly. The overlap distance is used to calculate a repulsive force using a “contact model” (Kloss et al., 2012)(Norouzi et al., 2016). At each time step, the normal and tangential contact forces are calculated on each particle, along with any other forces such as gravity. The particle positions at the next time step are then found using a numerical integration of Newton’s 2<sup>nd</sup> law of motion. The strength of DEM is that because particles are modeled at the individual particle level, it is in theory possible to accurately replicate all the physical phenomena of both particle mechanics and heat transfer (Goniva et al., 2010). The chief drawback of DEM is the high computational cost compared to continuum models. However, at current processing speeds, DEM is now viable for simulations of over 1 million particles, which is large enough to model a representative section of an actual device, as shown in this article. With continuous improvement in computer processing speeds, this approach promises to become even more advantageous in the coming decade.

In addition to modeling the mechanics of particle collisions, DEM can also perform heat transfer computations. Sub-models for each physical heat transfer mode have been developed, and several implementations have been described (Goniva et al., 2010)(Zhou et al., 2009). Modeling these heat transfer processes at the particle level is still relatively new, and when models are described in literature, they are often performed with in-house codes, such as those by Qi and Wright (2018) and Chaudhuri (2006).

There are several open source models available, such as LIGGGHTS and MFIX. Neither of these codes is very accessible for users trying to modify the models, as they are written in compiled languages and lack sufficient documentation and features. Specifically, LIGGGHTS has some

basic heat transfer models, but it is missing numerous important aspects: radiation is not available, the particle-fluid-particle and particle-fluid-wall modes (Section 3.4 and 3.5) are not implemented, boundary conditions are limited to a uniform temperature across the entire boundary mesh, and the contact conduction model may have an implementation error (Johnson, 2021a). The object oriented C++ code used for LIGGGHTS is highly optimized, but for those who are not already used to working with object oriented codes, it is not simple to implement new features. MFiX (Syamlal et al., 1993) is another potential option, but the user guide (MFS Development Group, 2021) offers no details about the particle-scale heat transfer models implemented, making it difficult to understand the physics or modify the underlying models, which are written in Fortran. Several commercial DEM codes also exist, but they have similar drawbacks and are not easily adaptable. These limitations may be part of the reason why engineers and researchers designing actual devices have been slow to adopt DEM-based heat transfer modeling.

A new open source DEM-based heat transfer model is described in this work to address some of these shortcomings, referred to as Dense Particle Heat Transfer (DPHT). It is developed for the special case of dense granular flows, which allows the particle mechanics (DEM) and heat transfer (DPHT) models to be kept separate, which simplifies the heat transfer modeling considerably; any DEM code can be used to model particle mechanics, and heat transfer is modeled separately with DPHT, with one-way coupling between the two models. Thus, the modeler only has to *use* the DEM software (not modify the source code), of which there are numerous optimized and computationally efficient options (e.g. LIGGGHTS, EDEM, Rocky). The modeler can focus on the heat transfer portion, DPHT, which is written in the Julia language (Bezanson et al., 2017). Julia has very fast computation speeds, approaching those of C++ (“Julia Micro-Benchmarks,” 2020), yet programming syntax is very simple, similar to interpreted languages such as Matlab or Python. Julia has compilation and parallelization built in, and it is free to use. The coupling scheme and the Julia code make DPHT much simpler to use and to modify compared to codes written in older compiled languages, where the DEM and heat transfer models integrated into a single code.

The sub-models for radiation are based on recent work by the authors (Johnson et al., 2021), and they have not been previously implemented in any DEM-based heat transfer code. The method

uses correlations to estimate Radiation Distribution Factors (RDFs), as a way to calculate radiative transfer between particles. It accurately accounts for radiation both between particles in contact and those separated by some distance, yet it is computationally efficient, adding little to the overall computation time.

One of the particle-particle radiation models found in literature is based on the local environment temperature around each particle. In this study, a simulation is set up to compare results from two different versions of the environment temperature model (Musser, 2011)(Krause et al., 2017) to the results of DPHT. In addition, a Monte Carlo ray tracing simulation is run to find the RDFs between all particles, providing a highly accurate solution to which the proposed models are compared.

Another significant gap in the literature is that few DEM-based heat transfer models have been experimentally validated, especially under the conditions of CSP, as there are few published data sets that have enough detail to perform such a validation. However, the solar receiver concept by Watkins (2018) provides one such data set, with experiments run under controlled laboratory conditions and with boundary conditions measured in many locations. Therefore, the DPHT model is run to simulate the exact conditions of the experiment, and the model is found to predict the experimental heat gain within 4%. This represents one important step forward in proving the validity of DPHT and other DEM-based heat transfer codes using the same sub-models.

This manuscript contains numerous contributions to the field of DEM-based modeling of heat transfer in granular flows. First, a comprehensive description of the six sub-models and their implementation is given for DPHT. Compared to other open source codes, DPHT offers a lower coding burden, giving flexibility to the modeler to implement new models or features in the future, even for engineers without experience in C++ or Fortran. The code is still computationally efficient, with DPHT only adding ~10% to the computation time of DEM alone, when a reasonable thermal time step is chosen (see Section 3.1). The particle-particle radiation model used in DPHT has not been implemented previously in any other DEM-based code. Moreover, it is shown to give more accurate results than two variants of the “local environment temperature” approach, which are shown to not conserve energy. In addition, the particle conduction models described have several improvements upon the models from literature. Next, to investigate the accuracy of the code for predicting behavior in a solar receiver, a DEM+DPHT

simulation is used to replicate the experimental work of Watkins (2018), with the close match indicating the validity of the code. Finally, a tubular heat exchanger is modeled, and a “radial” mixer is introduced, which is designed specifically to switch particles from the center with those near the walls. It shows extremely effective mixing, and it significantly increases heat transfer with the walls. Such an analysis shows the necessity of a DEM-based approach, as the continuum models often employed in CSP particle research (Watkins, 2018)(Albrecht and Ho, 2019)(Bartsch et al., 2016) cannot accurately simulate the mixing behavior of particles in such complex geometries.

The DPHT code is posted to an online repository (Johnson, 2021b), and a tutorial is available (Johnson, 2021a). To make it easy for others to adopt, the entire workflow (CAD modeling, mesh generation, DEM+DPHT modeling, visualization), is described using free or open source software. DPHT is intended for use in Ubuntu (Linux). DPHT is ready to model numerous heat exchangers and solar receivers using dense granular flows, and others are encouraged to download the source code and to share their work.

## **2. Assumptions and Applications**

The DPHT code is only valid for dense granular flows, as it is built on the assumption that the interstitial fluid has a negligible effect on the particle mechanics. Practically, this means only a DEM simulation is required to solve for the particle motion, not a coupled CFD-DEM simulation. Dense granular flows typically have solid fractions between 0.52 and the random packing limit of around 0.64 for uniformly sized spheres. In addition, it is assumed that the interstitial fluid can be considered stationary with respect to the particles, meaning no heat is transported away from the particles by convection. Heat transfer across the small fluid gap between particles is still modeled, but only as conduction through the stagnant fluid. Again, this avoids a coupled CFD-DEM simulation, which is much more computationally expensive. This approach also implies that the heat absorbed by the fluid is negligible compared to the heat absorbed by the particles, which is usually valid when the interstitial fluid is air. This same approach has been taken previously by Qi and Wright (2018) who studied a screw reactor and Chaudhuri et al. (2010) who studied rotary calciners.

As in most studies of small solid particles, each particle in DPHT is assumed to have a uniform temperature. This is a valid assumption if the particle is small and conductive enough that there is a small temperature difference across the particle, which corresponds to a Biot number much less than 1 (Grobbel, 2019). However, even for particles that do not strictly meet this criterion, the uniform particle temperature assumption could still be valid for dynamic simulations, as particles may move and rotate before a temperature gradient can form across the particle. While this behavior is theorized, it has not yet been studied in depth.

DPHT currently models spheres of uniform diameter, as most of the heat transfer sub-models implemented use this assumption. When a particle size distribution is known from experiments, the Sauter mean diameter is often used as the particle diameter (Grobbel, 2019).

The Distance Based Approximation (DBA) radiation model was derived using Monte Carlo ray tracing through groups of spherical-shaped particles, under the assumptions of gray, diffuse reflections and emissions (Johnson et al., 2020). That study relied on geometric optics where diffraction and near-field effects are neglected, which is a valid assumption for particles greater than 75  $\mu\text{m}$  (Bouvard and Argento, 1996)(Tien, 1988), and therefore the radiation model may not be applicable for smaller particles. The DBA model relies on tables of radiation distribution factors generated with Monte Carlo ray tracing. Tables have been generated for particle emissivities of 0.86 and 0.65 (corresponding to sintered bauxite and sand, respectively), and wall emissivities of 0.40, 0.60, 0.80, and 1.0 (Johnson et al., 2021). For other wall emissivities, the tables can be interpolated, but for different particle emissivities, new tables would need to be generated, following the procedure described in detail (Johnson et al., 2021).

In the field of CSP, numerous solid particle solar receivers and heat exchangers have been proposed which use a dense granular flow, for which the DPHT code is applicable. Several notable examples include solar receivers with gravity-driven flow through metal tubes, (Watkins, 2018)(Johnson et al., 2017)(Johnson, 2021a), a particles-to-supercritical  $\text{CO}_2$  heat exchanger designed by Sandia National Laboratory (Albrecht and Ho, 2019), and a “moving bed heat exchanger” studied by researchers at the German Aerospace Center (Bartsch et al., 2016)(Baumann and Zunft, 2015). Other examples include the CentRec solar receiver (Hicdurmaz et al., 2020), and the recently-proposed transparent tubular solar receiver (Niederwestberg et al., 2020). In the hexagonal tube receiver by the National Renewable Energy



Laboratory (Morris et al., 2016), the flow is not strictly dense, but DPHT may still be applicable since particles are not entrained in air. Outside of the CSP industry, other possible uses include static powder beds used for laser sintering (Gusarov, 2020) and rotating kilns (Chaudhuri et al., 2006). Each of these examples could have been modeled with DPHT, either with the current capabilities of the code, or after some modifications. In most of these studies, continuum approximations were made to perform the modeling, given the few available DEM-based options. In contrast to the examples mentioned, DPHT is not applicable when particles are falling through air or fluidized, as particle-fluid convection is significant in these cases.

### **3. Model Details**

#### **3.1. Coupling of DEM and DPHT**

To run a coupled DEM+DPHT simulation, a DEM simulation is first run to find the particle positions at each time step, with no heat transfer calculations performed. Text files containing the xyz particle positions are output throughout the DEM simulation. LIGGGHTS is used in this work, but any similar DEM code would work as well. After the DEM simulation has finished, DPHT reads the particle position files, and heat transfer is calculated between each particle and every other nearby particle and the wall. The combination of DEM and DPHT can be considered a “one-way” coupling, where information only flows from the DEM model to the DPHT model. The benefit of this scheme is that after running the DEM simulation once to find the particle positions over time, multiple thermal simulations can be run to investigate different thermal parameters (e.g. temperature boundary conditions, or particle thermal conductivity), without having to run the DEM simulation again, which often takes the vast majority of the total simulation time. The disadvantage of one-way coupling is that the mechanics cannot be modified based on thermal information, such as having temperature-dependent particle friction properties. These properties are often not known so this is not a large drawback.

Most DEM implementations require the time step size to be small enough that multiple time steps occur throughout a single collision, called the “soft-sphere” approach. Acceptable time step sizes are limited by the Rayleigh and Hertz time steps (Grobbel, 2019), resulting in time step sizes often in the range of  $10^{-5}$  to  $10^{-6}$  seconds. Heat transfer can be calculated much less

frequently than the particle mechanics, so the particle position files are only written at a specified interval, forming a “thermal time step”. For example, in Section 4, DPHT uses a thermal time step size of 2000 DEM time steps, which is shown to be sufficiently small.

When DPHT runs, it reads the xyz position of every particle at the current time step. For each particle (generally referred to as particle  $i$ ), it iterates through all other ( $j$ ) particles, first calculating the particle-particle (PP) distance, termed  $d_{ij}$  in the sections that follow. If  $d_{ij}$  is less than a specified cutoff distance, the PP heat transfer calculations are performed using the heat transfer sub-models described in Sections 0, 3.4, and 3.6. If particle  $i$  is near a wall, the particle-wall (PW) heat transfer is found using the sub-models described in Sections 3.3, 3.5, and 3.7, where the temperature of the wall is taken to be that of the closest wall element. The net heat transfer rate from particle  $i$  to all other  $j$  particles and the wall is found, and temperature of particle  $i$  at the next time step is found with the conservation of energy using Eq. (1). In this equation,  $m$  is the particle mass,  $C_p$  is the particle specific heat,  $q_{net,i}$  is the net heat transfer rate to particle  $i$  and  $\Delta t_{thermal}$  is the thermal (DPHT) time step.

$$T_{i,next} = T_{i,current} + \frac{q_{net,i} \Delta t_{thermal}}{m C_p} \quad (1)$$

The six sub-models for heat transfer are shown in Figure 1 and described in the following sections.

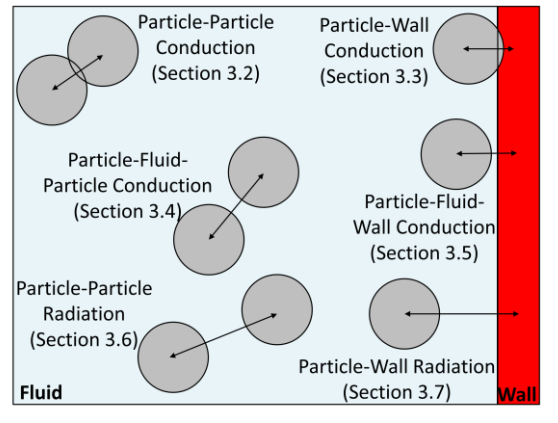


Figure 1. The six heat transfer modes modeled in DPHT.

### 3.2. Particle-Particle Conduction

The particle-particle (PP) conduction model, shown in Eq. (2), accounts for heat conduction through the circular contact area between two touching particles. The model was originally developed by Batchelor and O'Brien (1977), and the "artificial softening factor" ( $c_{PP}$ ) was later added by Zhou et al. (2010). The original form and the form by Zhou et al. have been implemented by several researchers (Chaudhuri et al., 2006)(Qi and Wright, 2018)(Kloss et al., 2012)(Zhou et al., 2009). The particle temperatures are  $T_i$  and  $T_j$ , the thermal conductivity of the solid material is  $k_s$ , the contact radius is  $r_c$ , and the dimensions of two overlapping particles are shown in Figure 2. The artificial softening factor is needed because a typical practice in DEM modeling is to use a Young's modulus value several orders of magnitude lower than the actual value, allowing for a larger time step and quicker simulations. This softening has the undesired side effect of increasing the contact area in heat transfer calculations. The factor  $c_{PP}$  compensates for this by using the ratio of the real Young's modulus to the one used in the DEM simulation (Zhou et al., 2010). Equation (2) was originally derived for particles in static contact, though it has been used widely for dynamic calculations as well (Chaudhuri et al., 2010)(Oschmann et al., 2016)(Zhou et al., 2009)(Cheng et al., 1999). In the DPHT model, the PP distance ( $d_{ij}$ ) is known, and the contact radius is found with Eq. (4).

$$q_{PP,cond} = 2 c_{PP} k_s r_c (T_i - T_j) \quad (2)$$

$$c_{PP} = \left( \frac{Y_{DEM}}{Y_{real}} \right)^{1/5} \quad (3)$$

$$r_c = \sqrt{R^2 - \left( \frac{d_{ij}}{2} \right)^2} \quad (4)$$

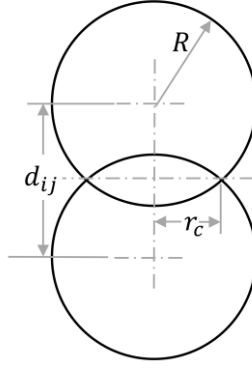


Figure 2. Geometry of two contacting spheres used to calculate particle-particle conduction.

### 3.3. Particle-Wall Conduction

The particle-wall (PW) conduction model is essentially the same as the PP conduction model of Eq. (2), with several modifications. The contact radius  $r_c$  is found with Eq. (5), where  $R$  is the particle radius and  $d_{iw}$  is the distance from the particle center to the wall.

$$r_c = \sqrt{R^2 - d_{iw}^2} \quad (5)$$

The particle and wall thermal conductivities are combined to form an effective conductivity incorporating both the particle conductivity ( $k_{si}$ ) and the wall conductivity ( $k_{sw}$ ), following the method from Cheng et al. (1999).

$$q_{PW,cond} = \frac{4}{\frac{1}{k_{si}} + \frac{1}{k_{sw}}} c_{PW} r_c (T_i - T_w) \quad (6)$$

For PW heat transfer, the artificial softening factor is calculated with Eq. (7), which is interpreted from Zhou et al. (2010) for the case where particles  $i$  and  $j$  have different properties. The Poisson's ratios are  $\nu_i$  and  $\nu_j$  respectively,  $Y_{i,DEM}$  and  $Y_{j,DEM}$  are the Young's moduli used in the DEM simulation, and  $Y_{i,real}$  and  $Y_{j,real}$  are the Young's moduli of the real materials. In this case, the particle  $j$  is taken to be the wall.

$$c_{PW} = \left( \frac{\left( \frac{1 - v_i^2}{Y_{i,real}} \right) + \left( \frac{1 - v_j^2}{Y_{j,real}} \right)}{\left( \frac{1 - v_i^2}{Y_{i,DEM}} \right) + \left( \frac{1 - v_j^2}{Y_{j,DEM}} \right)} \right)^{1/5} \quad (7)$$

### 3.4. Particle-Fluid-Particle Conduction

The heat conducted across the stagnant fluid gap between two nearby particles is often the leading mode of heat transfer in dense granular flows found in CSP heat exchangers. This particle-fluid-particle (PFP) conduction mode exists both for particles in contact and those which are close but not actually touching. In the original derivation by Cheng et al. (1999), a ‘‘Voronoi’’ polyhedron is constructed around each particle, resulting in a polygon surface drawn between all particles. To analyze the heat transfer between two particles, a volume is created by connecting the vertices of the shared polygon with the centers of the particles. Since such a volume has no analytical heat transfer solution, the volume is then replaced by two opposing cones of the same volume, which share their base areas and have points at the particle centers. A diagram showing the cone geometry is shown in Figure 3(a) for non-contacting particles and in Figure 3(b) for contacting particles, where orange lines designate the outlines of the cones.

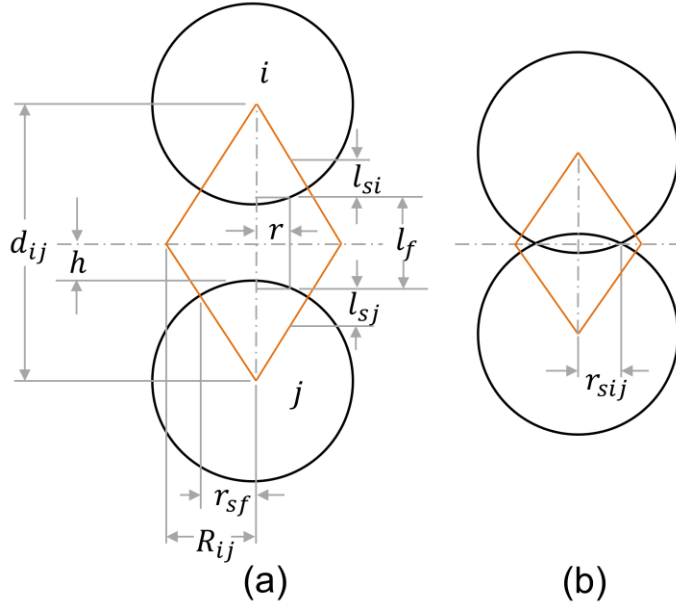


Figure 3. A 2D representation of the sphere and cone geometry (Cheng et al., 1999), with dimensions corresponding to Eq. (8), for (a) non-contacting and (b) contacting spheres. Outline of the double cone volume is shown in orange.

The opposing cone configuration allows for an analytical calculation of heat transfer to particle  $i$  from particle  $j$  using a conduction resistance approach, where heat flux is assumed to be parallel to the vector between particle centers. The surfaces of the two cones are considered isothermal at  $T_i$  and  $T_j$ . The original form given by Cheng et al. (1999) has been rearranged to form Eq. (8), showing three resistances to heat conduction: through the solid of particle  $i$  a length of  $l_{si}$ , through the fluid a length of  $l_f$ , and through particle  $j$  a length of  $l_{sj}$ . These lengths depend on the radial position ( $r$ ) and are found with Equations (9) and (10). In these equations,  $R$  is the particle radius,  $R_{ij}$  is the cone base radius, and  $h$  is the distance from the center plane to the closest “tip” of the particle, found with Eq. (11). In Eq. (8), the term  $\left(\frac{l_{si}}{k_{si}} + \frac{l_f}{k_f} + \frac{l_{sj}}{k_{sj}}\right)^{-1}$  gives the heat flux as a function of the radial position,  $r$ . This is multiplied by the circular differential area  $2\pi r dr$  and integrated over the radial position  $r$ . After multiplying by the temperature difference, this gives the total heat transfer rate from particle  $i$  to particle  $j$ . Because particles are assumed to have a uniform diameter in DPHT, the distance through the solid is the same for each sphere ( $l_{si} = l_{sj}$ ). The lower integration limit ( $r_{sij}$ ) is taken as zero for non-contacting particles and as the contact

radius ( $r_c$ ) for overlapping particles. The upper integration limit ( $r_{sf}$ ) represents the intersection of the cone and the sphere, calculated with Eq. (12).

$$q_{PPF,i,j} = (T_j - T_i) \int_{r_{sij}}^{r_{sf}} \left( \frac{l_{si}}{k_{si}} + \frac{l_f}{k_f} + \frac{l_{sj}}{k_{sj}} \right)^{-1} 2\pi r dr \quad (8)$$

$$l_{si} = l_{sj} = \sqrt{R^2 - r^2} - \frac{r(R + h)}{R_{ij}} \quad (9)$$

$$l_f = 2 \left[ (R + h) - \sqrt{R^2 - r^2} \right] \quad (10)$$

$$h = \frac{d_{ij} - 2R}{2} \quad (11)$$

$$r_{sf} = \frac{R_{ij}R}{\sqrt{R_{ij}^2 + (R + h)^2}} \quad (12)$$

$$R_{ij} = 0.560R\alpha_s^{-1/3} \quad (13)$$

In the original formulation by Cheng et al., the cone base radius ( $R_{ij}$ ) term was calculated from the Voronoi polyhedra drawn around all particles at each time step, a very computationally expensive process. To eliminate this requirement, Zhou et al. (2009) interpreted the results from Yang et al. (2002) to express the cone base radius as a function of only the particle radius and solid fraction ( $\alpha_s$ ). With this advancement,  $R_{ij}$  can be found using Eq. (13), eliminating the need to build any Voronoi polyhedra.

Instead of solving Eq. (8) within the main DPHT code at each time step and for each particle pair, it is much more computationally efficient to use pre-calculated heat transfer coefficients (HTC), where the HTC is only the integral part of Eq. (8). This is done by numerically solving the integral for many combinations of particle distance ( $d_{ij}$ ) and temperature. Though temperature is not a term in the integral portion of Eq. (8), the thermal conductivity of air ( $k_f$ ), and therefore the HTC, is strongly temperature dependent. At the beginning of a simulation, a set of temperatures (ranging from 0 to 1000 °C) and a set of  $d_{ij}$  distances (ranging from 1.6 to 3.1 radii) are identified as the relevant ranges of these variables. The HTC is solved for each combination of temperature and PP distance, and the resulting HTC values are stored in a matrix.

During the simulation, when calculating PFP conduction between any two particles, the applicable HTC value is found using a bilinear interpolation of the HTC matrix over  $d_{ij}$  and the temperature, where the HTC is evaluated at  $(T_i + T_j)/2$ . The HTC value is then multiplied by  $(T_j - T_i)$  to find the PFP conduction in Watts. Calculated HTC values for air are shown as a function of distance and temperature in Figure 4. According to Zhou et al. (2009), heat transfer becomes negligible for  $\frac{h}{R} > 0.5$ , or equivalently,  $d_{ij} > 3R$ . The HTC (Figure 4) indeed becomes low at distances greater than  $3R$  for low temperatures, however, for high temperatures a higher cutoff distance may be necessary, as the curve for 1273 K still shows 7% of its peak value this distance. In the analyses that follow, PFP heat transfer was neglected above  $3R$ , since particle temperatures are well below 1273 K. A temperature dependent thermal conductivity of the particle is currently not included in DPHT because such data is not available in literature for sand or sintered bauxite, the leading materials for particle-based CSP.

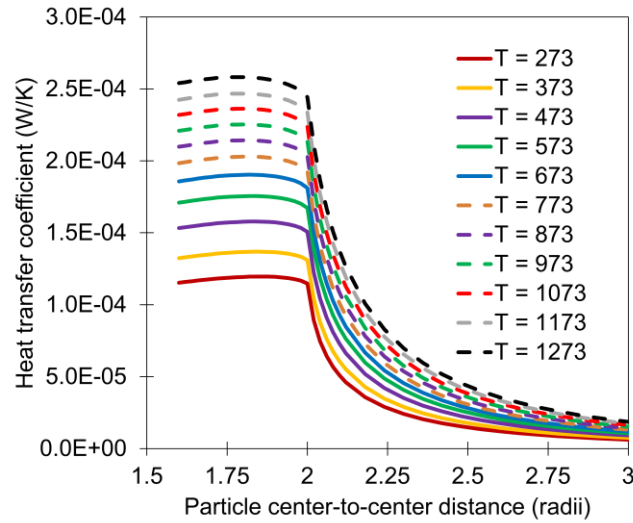


Figure 4. Particle-fluid-particle heat transfer coefficients solved for air at various temperatures (K). Particle properties:  $k_{si}=k_{sj}=2.0$ ,  $\alpha_s = 0.60$ , and  $R=5e-4$  m.

Similar to PP and PW conduction, the true distance between two contacting particles is less than it is in the DEM simulation because of the artificially low Young's modulus. The literature did not show a correction factor for PFP conduction, so one is derived to relate the center-to-center distance within the DEM simulation ( $d_{ij,DEM}$ ) to a corrected distance ( $d_{ij,real}$ ) after



compensating for the artificial softening. From the geometry of two overlapping spheres (referring back to Figure 2), Equations (14) and (15) relate the particle radius ( $R$ ), the distance ( $d_{ij}$ ), and contact radius ( $r_c$ ) for both the real and DEM cases. Equation (16) is another expression of the same  $c_{PP}$  factor used previously in Eq. (3) from Zhou et al. (2010) which relates the true and DEM-modeled contact radii.

$$R^2 = (d_{ij,DEM}/2)^2 + r_{c,DEM}^2 \quad (14)$$

$$R^2 = (d_{ij,real}/2)^2 + r_{c,real}^2 \quad (15)$$

$$c_{PP} = \frac{r_{c,real}}{r_{c,DEM}} \quad (16)$$

Substituting and rearranging these three equations, the real distance can be found in terms of the DEM-modeled distance, the radius, and  $c_{PP}$ , to form Eq. (17). This corrected distance ( $d_{ij,real}$ ) is then used in the bilinear interpolation of the HTC. Using  $d_{ij,real}$  instead of  $d_{ij,DEM}$  has the effect of making contacting particles further away from each other, reducing PFP conduction heat transfer. For non-contacting particles, the distance correction with Eq. (17) does not apply, and  $d_{ij,real} = d_{ij,DEM}$ .

$$d_{ij,real} = 2\sqrt{R^2 - c_{PP}^2 \left[ R^2 - (d_{ij,DEM}/2)^2 \right]} \quad (17)$$

### 3.5. Particle-Fluid-Wall Conduction

The particle-fluid-wall (PFW) conduction model for DPHT is developed by following a similar derivation as the PFP model, with the geometry adapted to a particle-wall configuration. As shown in Figure 5, the surface of the wall is specified as  $T_w$ , so there is no heat transfer resistance due to the wall itself (i.e. heat does not have to conduct into the wall any distance to reach the specified  $T_w$ ). Thus, as shown in Figure 5, there are only conduction resistances due to the fluid (through a distance of  $l_f$ ) and the particle (through a distance of  $l_{si}$ ). This is in contrast to the model from previous researchers (Qi and Wright, 2018), which included a conduction resistance of the wall. Equations (11)-(13) from the PFP conduction section are used for  $h$ ,  $r_{sf}$ , and  $R_{ij}$ . Note that  $l_f$  in this context is half of the value used in PFP conduction.

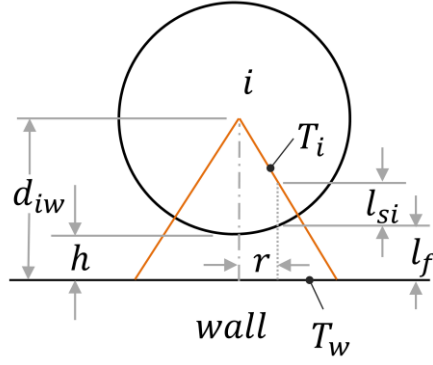


Figure 5. Particle-fluid-wall geometry.

$$q_{PFW,iw} = (T_w - T_i) \int_{r_{sij}}^{r_{sf}} \left( \frac{l_{si}}{k_{si}} + \frac{l_f}{k_f} \right)^{-1} 2\pi r dr \quad (18)$$

$$l_{si} = \sqrt{R^2 - r^2} - \frac{r(R + h)}{R_{ij}} \quad (19)$$

$$l_f = (R + h) - \sqrt{R^2 - r^2} \quad (20)$$

When a particle overlaps the wall, the overlap distance in DEM is greater than it should be, due to the artificially low Young's modulus used for both the particles and the wall. Equations (21) to (23) give the relations between particle radius ( $R$ ), the particle-wall distance ( $d_{iw}$ ), and contact radius ( $r_c$ ) for both the DEM and real cases. The two cases are related through the factor  $c_{PW}$ , this time using Eq. (7) as the wall and particle materials are different. After substitutions, the real PW distance ( $d_{iw,real}$ ) is found from the known variables with Eq. (24).

$$R^2 = d_{iw,DEM}^2 + r_{c,DEM}^2 \quad (21)$$

$$R^2 = d_{iw,real}^2 + r_{c,real}^2 \quad (22)$$

$$c_{PW} = \frac{r_{c,real}}{r_{c,DEM}} \quad (23)$$

$$d_{iw,real} = \sqrt{R^2 - c_{PW}^2 [R^2 - d_{iw,DEM}^2]} \quad (24)$$

Similar to PFP conduction, at the beginning of the DPHT simulation, Eq. (18) is numerically integrated to solve for the PFW heat transfer coefficient at many combinations of PW distance

and temperature. Again, these are saved in a matrix, which is interpolated when calculating PFW conduction between each particle  $i$  and the wall. The temperature used in the interpolation is the mean temperature of the particle and the nearest wall element. The PW HTC curves for air as the interstitial fluid are shown in Figure 6.

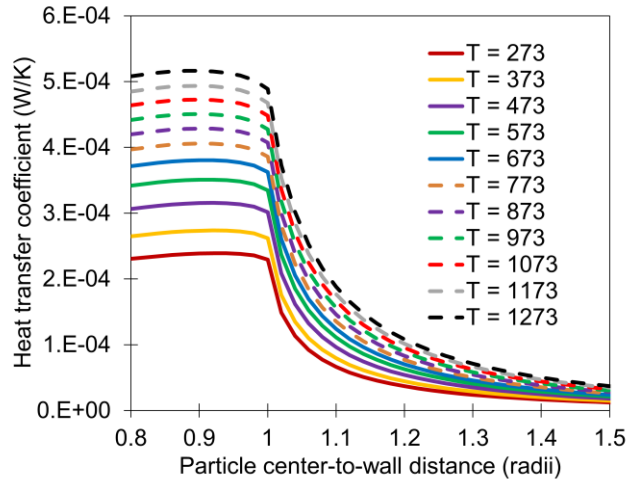


Figure 6. Particle-fluid-wall heat transfer coefficients solved for air at various temperatures (K). Particle properties:  $k_{si}=2.0$ ,  $\alpha_s = 0.60$ ,  $R=5e-4$  m.

### 3.6. Particle-Particle Radiation

The Distance Based Approximation (DBA) radiation model is implemented for PP radiation, which was previously developed by the authors (Johnson et al., 2021). In the creation of the DBA model, Monte Carlo ray tracing simulations were run to find the average Radiation Distribution Factor (RDF) between two particles inside a particle bed, at various PP distances. The RDF from one particle to another is the ratio of rays (photons) absorbed by the second particle to the total number of rays emitted, after any number of reflections off surrounding particles. The RDF incorporates reflections, unlike the more common radiative view factor. The Monte Carlo simulations resulted in curves to estimate the RDF based on the PP distance. These curves were found for various solid fractions (0.25, 0.35, 0.45, 0.55, and 0.64) and two particle emissivities (0.65 and 0.86), and saved in table format. To simulate particles with an emissivity other than 0.65 or 0.86, new PP RDF tables would have to be developed.

Within DPHT, the RDF between two particles is estimated with a bilinear interpolation over the solid fraction and PP distance. Separate solid fractions for the near-wall region and for the bulk region have been used, as the solid fraction changes slightly near the wall (Johnson et al., 2021). These solid fractions must be calculated externally and specified before the simulation is run. If the solid fraction varies in different regions of the domain, the solid fraction would need to be specified for the different regions or calculated locally around each particle. After interpolation to find the RDF, the heat transfer rate from particle  $j$  to particle  $i$  is found with Eq. (25), where  $\varepsilon_p$  is the particle emissivity,  $A_p$  is the surface area of one particle,  $\sigma$  is the Stefan-Boltzmann constant,  $D_{ij}$  is the RDF, and  $T$  is the absolute temperature.

$$q_{rad,ij} = \varepsilon_p A_p \sigma D_{ij} (T_j^4 - T_i^4) \quad (25)$$

### 3.7. Particle-Wall Radiation

The DBA model has another set of RDF curves for estimating the RDF between a particle and the wall (Johnson et al., 2021). For PW radiation, the wall emissivity is also incorporated into the tabulated RDF curves, leading to a table for each combination of solid fraction (0.25, 0.35, 0.45, 0.55, and 0.64), particle emissivity (0.65 and 0.86), and wall emissivity (0.4, 0.6, 0.8, and 1.0). In DPHT, the PW RDF is estimated using the applicable table and a bilinear interpolation over the PW distance and the solid fraction. The PW radiative transfer rate is found with Eq. (26), where  $D_{iw}$  is the RDF from particle  $i$  to the wall, and  $T_w$  is the temperature of the closest wall element. Note that the wall emissivity does not appear in the equation, but its effect is taken into account in the Monte Carlo modeling and the development of the RDF tables.

$$q_{rad,iw} = \varepsilon_p A_p \sigma D_{iw} (T_w^4 - T_i^4) \quad (26)$$

### 3.8. Thermal Boundary Conditions

There are two options for boundary conditions currently implemented in DPHT: Dirichlet (specified wall temperature) and adiabatic.

To specify the wall temperatures, the mesh information is read in to DPHT at the beginning of the simulation, and each element is assigned a temperature. The temperature is specified using the coordinates of the element centroid, allowing for any desired temperature profile such as a uniform wall temperature or a polynomial. For PW heat transfer, the closest wall element to the particle is identified based on the wall element centroid, as shown in red in Figure 7, and heat transfer is calculated using the perpendicular wall distance ( $d_{iw}$ ) in the PW heat transfer models. More detailed information on applying boundary conditions is available (Johnson, 2021a).

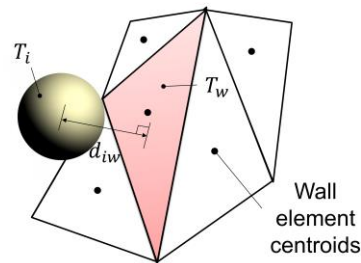


Figure 7. Particle and wall element geometry used for applying boundary conditions.

The other boundary condition option is to specify wall elements as adiabatic, meaning no PW heat transfer is calculated with these elements. This is especially useful in certain situations such as heat exchanger design, where insulated inlet and outlet sections are desired. Unlike in CFD, specifying a non-zero heat flux at a boundary is not straightforward, as heat would need to be distributed among the near-wall particles.

In addition to walls, heat transfer with the surroundings may occur via other boundary conditions, such as free convection to the fluid above a static bed or radiation striking particles directly, which may be important in the case of a solar receiver such as CentRec (Hicdurmaz et al., 2020). These are not implemented into DPHT, but they could be added as heat source terms once an applicable model is developed.

## 4. Direct Comparison of Particle-Particle Radiation Models

Particle-particle radiation is implemented in DPHT using the Distance Based Approximation (DBA) radiation model (Johnson et al., 2021). In this section, simulations are run to compare the

DBA model with the “environment temperature” methods described by Musser (2011) and Krause et al. (2017). Additionally, a Monte Carlo ray tracing simulation is performed for each particle in the bed, so the Radiation Distribution Factor (RDF) between all particles is known to a very high accuracy. Therefore, the Monte Carlo model gives a solution to which the three radiation models can be compared.

The simulation uses a packed bed of 17563 particles, with a radius of 500 microns, an emissivity of 0.65, and a solid fraction of 0.58. For the simulation, all particles with centers having  $x > 0.004$  are maintained at 1000 °C, particles with  $x < -0.004$  are maintained at 650 °C, and particles in between are allowed to change temperature until a steady state is reached, as shown in Figure 8. All other PP heat transfer modes are neglected, so the only heat transfer is due to PP radiation. The results from the different models are compared in terms of the total heat transfer rate from the hot region to the cold region.

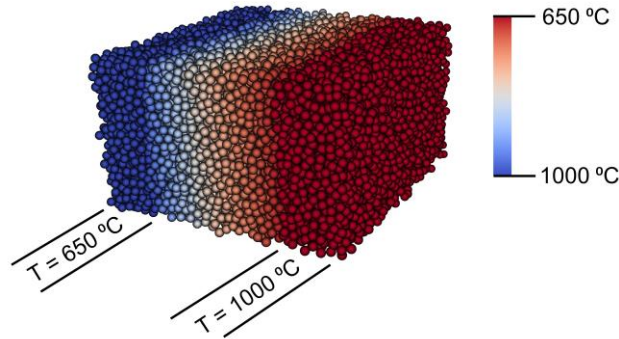


Figure 8. Static particle bed used for comparing different particle-particle radiation models. Temperatures shown are found with the DBA model.

The model described by Musser (2011) uses the local environment temperature ( $T_{env}$ ) around each  $i$  particle, which is taken to be the average temperature of all other particles within a distance of 3 radii (center-to-center), shown in Eq. (27).  $T_j$  is the temperature of each neighboring particle  $j$ , and  $n_j$  is the number of  $j$  particles within 3 radii. Radiative transfer to particle  $i$  ( $q_{rad,i}$ ) is calculated with Eq. (28), where  $\varepsilon_p$  is the particle emissivity,  $A_p$  is the particle surface area,  $\sigma$  is the Stefan-Boltzmann constant, and  $T_i$  is the temperature of particle  $i$ .

$$T_{env} = \frac{1}{n_j} \sum_{j=1}^{n_j} T_j \quad (27)$$

$$q_{rad,i} = \varepsilon_p A_p \sigma (T_{env}^4 - T_i^4) \quad (28)$$

A similar model to find the local environment temperature is described by Krause et al. (2017), which reduces to Eq. (29) after assuming a constant particle radius and emissivity.

$$T_{env}^4 = \frac{1}{n_j} \sum_{j=1}^{n_j} T_j^4 \quad (29)$$

The fourth model uses the RDFs found with a Monte Carlo ray tracing simulation. The RDFs between each particle and every other particle are found using the open source code also published by the authors (Johnson, 2021c). This code traces gray, diffuse rays emitted from the surface of each particle to calculate the RDFs, which incorporates reflections off surrounding particles. In the current simulation,  $10^5$  rays are emitted from the surface of each particle, which has been shown to be sufficient for high accuracy (Johnson et al., 2020). The output of the ray tracing simulation is a matrix with dimensions of 17563 by 17563, containing the RDF from each particle to every other particle in the domain. In the DPHT simulation, the RDF between each particle  $i$  and every other particle  $j$  is found by looking up the value in this matrix, and the radiative transfer is found using, Eq. (25), similar to the DBA model but with the RDF known with a high accuracy. The Monte Carlo simulation is useful because it provides an accurate solution to which these PP radiation models can be compared, but it is much too computationally expensive to implement in DPHT for dynamic systems. It is feasible for simulations such as this test case, where particles are static.

Each of the four models is implemented in DPHT, and the simulations are run until a steady state is reached. The initial temperatures of the particles in the central region are specified using a linear interpolation between the hot and cold regions, which enables the simulation to establish a steady state after a relatively short period of time. At each time step, the rate of heat leaving the hot region and the rate of heat entering the cold region are output from the simulation, and a steady state is reached once these values converge. Figure 9 shows how each of the four models

evolves toward the steady state, with several interesting results found. First, the DBA model tracks the actual Monte Carlo simulation extremely well, with the steady state heat transfer differing by only 1.6%. The model described by Krause et al. (2017) nearly converges, but it underestimates the total heat transfer by 15%. The model by Musser (2011) actually never converges, meaning that the heat transferred from the hot region is always more than is absorbed by the cold region, which is physically unreasonable.

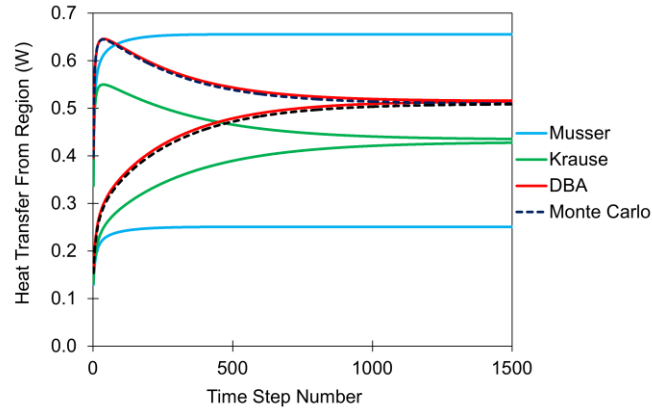


Figure 9. Heat transfer rate from the hot region (top curves) and to the cold region (lower curves) for the four particle-particle radiation models compared.

The reason for the mismatch is that the environment temperature methods do not guarantee conservation of energy. The quantity of heat transferred to particle  $i$  is a function of the temperatures of the surrounding particles, but there is no way to ensure that the same amount of heat absorbed by particle  $i$  is removed from the surrounding particles. In contrast, the DBA and Monte Carlo methods compute heat transfer between each pair of particles; the same amount of heat is simultaneously added to particle  $i$  and subtracted from particle  $j$ , ensuring that no heat is gained or lost. To investigate this further, the net heat transfer rate across all particles is summed at each time step, which should equal zero if energy is conserved. As expected, the DBA and Monte Carlo methods are each found to have a net heat transfer of zero. The method of Musser has a value of  $-0.404$  W, meaning the conservation of energy is violated, and the total energy in the group of particles decreases with time in a physically unrealistic way. The error is extremely large, considering the total heat transfer from hot to cold regions is  $0.509$  W, calculated with the



Monte Carlo method. The model by Krause et al. also does not guarantee conservation of energy, but the energy loss is less severe, at 0.0048 W. These results are summarized in Table 1.

Table 1. Results comparing four particle-particle radiation models.

	Musser	Krause	DBA	Monte Carlo
Steady state heat transfer rate (W)	Not Converged	0.432	0.515	0.509
Error in steady state heat transfer (with respect to Monte Carlo)	-	-15.3%	1.6%	-
Erroneous heat generation at steady state (W)	-0.404	-0.0048	0	0

This analysis shows how each of the PP radiation models computes heat transfer under identical conditions, and the DBA model shows closest match to the Monte Carlo solution. The model from Musser is shown to give extremely unrealistic results, with a high rate of energy disappearing. The model of Krause et al. underestimates heat transfer by 15% in this case, but the error may change with factors such as the temperature gradient, the solid fraction, and the emissivity. Both of the environment temperature models should be treated with care as they do not conserve energy. The temperature gradient modeled is relatively severe, which may accentuate some of these discrepancies, but the temperature gradient is realistic for a CSP heat exchanger in dense granular flow, as shown in Section 5. Such a detailed validation is possible because the Monte Carlo ray tracing code was specifically built in previous work for these types of simulations, whereas the creators of the previous models may not have had such a tool available.

The DBA model has been developed to provide a more accurate model for radiation, compared to current methods, while still maintaining a low computational cost compared with a full Monte Carlo simulation. The computational benefit of the DBA model is clear, as an accurate Monte Carlo simulation to find all the RDFs in a bed of 50,000 particles may take hours of run-time, while the DBA model approximates the RDFs in seconds. Outside the ranges of particle emissivity, wall emissivity, and solid fraction for which the DBA model was developed, new distance vs. RDF curves could be found, with results tailored for the conditions of interest (Johnson et al., 2021).

In this section, the different radiation models were compared to the Monte Carlo model under the assumptions of an idealized system, with particles being uniformly sized spheres having gray and

diffuse emissions and reflections. A real system would not exactly match these assumptions, so experimental validation of these radiation models would be useful future work. In addition, the radiation models should be compared in the future under more complex conditions, such as near walls or at the surface of the particle bed, as well as in beds where the solid fraction varies across the domain.

## **5. Comparison with Experimental Data**

Very few studies have attempted to compare or validate DEM-based heat transfer models with experimental data of dense granular flows, especially under the conditions relevant for CSP. Recently, DPHT simulations were compared against experiments under a high flux solar simulator, where a deviation between 0 and 9% was found in terms of overall heat transfer (Johnson, 2021a). To continue building the case for the accuracy of this modeling approach, the present study focuses on an experiment performed by Watkins (2018), which provides a useful test case for DPHT. In this experiment, particles descend through an ohmically heated Inconel tube. As shown in Figure 10, the hopper supplies the tube with particles, and an orifice plate is located at the outlet, ensuring a dense granular flow throughout the setup. Particles in this experiment are zirconia-silica, with a diameter of 320  $\mu\text{m}$ . The properties used in the DEM+DPHT simulation are shown in Table 2. The particle diameter, specific heat, density, mass flow rate, and boundary conditions are specified by Watkins (2018), while the other properties are chosen to be the closest values possible given the available literature. No calibration of the mechanical DEM parameters has been done for zirconia-silica, so the properties of sintered bauxite particles are used (Grobbel, 2019). This test is referred to as Configuration 6 by Watkins (2018).

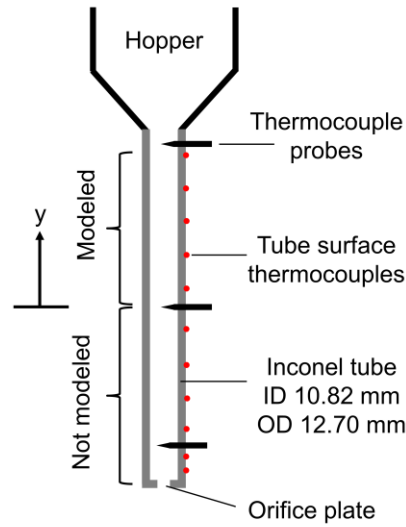


Figure 10. Experimental setup used by Watkins (2018) and modeled in the present study.

Table 2. Properties used in DEM+DPHT simulation (P=particle, W=wall).

Parameter	Value
Number of particles	$2.35 \times 10^6$
Inner diameter	10.82 mm
Outer diameter	12.70 mm
DEM time step size	$5 \times 10^{-6}$ s
DPHT (thermal) time step size	0.01 s
Particle diameter	320 $\mu$ m
Particle temperature at inlet	30 $^{\circ}$ C
Initial particle temperature	30 $^{\circ}$ C
Mass flow rate	$0.00288 \text{ kg s}^{-1}$
Particle Material Density	$3800 \text{ kg m}^{-3}$
Poisson's Ratio, P	0.30
Poisson's Ratio, W	0.30
Coefficient of sliding friction, PP	0.72
Coefficient of sliding friction, PW	0.30
Coefficient of rolling friction, PP	0.13
Coefficient of rolling friction, PW	0.50
Coefficient of restitution, PP	0.82
Coefficient of restitution, PW	0.44
Thermal conductivity, P	$2.1 \text{ W m}^{-1} \text{ K}^{-1}$
Thermal conductivity, W	$14.5 \text{ W m}^{-1} \text{ K}^{-1}$
Specific heat capacity, P	$271.5 T^{0.1719} \text{ J kg}^{-1} \text{ K}^{-1}$ ( $T$ in $^{\circ}$ C)
Emissivity, P	0.65
Emissivity, W	0.60
Young's Modulus, DEM, P	$5 \times 10^6 \text{ N m}^{-2}$
Young's Modulus DEM, W	$5 \times 10^6 \text{ N m}^{-2}$
Young's Modulus, real, P	$205 \times 10^9 \text{ N m}^{-2}$
Young's Modulus, real, W	$200 \times 10^9 \text{ N m}^{-2}$
Solid Fraction, bulk	0.6124
Solid Fraction, near wall	0.5405

The mean particle temperature is reported by Watkins at the inlet and at distances of 0.645 m and 1.27 m from the inlet. To reduce the computational cost of the simulation, only the top half of the setup was modeled in the present study (above  $y = 0$  in Figure 10), so the mean temperature measurement at 1.27 m was not used.

The tube temperatures were measured with thermocouples affixed to the outside of the tube wall, whereas the wall temperatures on the *inside* of the tube wall are needed for the DPHT simulation. In (Watkins, 2018), this temperature difference was calculated to be 3.1 °C at 0.645 m from the inlet, so the inner tube temperature was set as 3.1 °C lower than the outside tube temperature for each of the measured points. These adjusted wall temperature measurements are shown in Figure 11. A curve fit was applied to these points, resulting in Eq. (30), which gives the inner wall temperature ( $T_w$ ) in Kelvin as a function of the  $y$  coordinate in meters. The wall temperature in DPHT was specified using this equation and is shown as the dashed blue line in Figure 11.

$$T_w = -995.70y^3 + 381.44y^2 - 657.96y + 1057.8 \quad (30)$$

In the DEM simulation, the diameter of the orifice at the outlet was modified until the flow rate matched that of the experiment,  $0.00288 \text{ kg s}^{-1}$ . The boundaries at  $y=0$  m and  $y=0.66$  m were specified as periodic in LIGGGHTS, so particles at the bottom boundary immediately reappear at the top boundary, with the same velocity and  $x$ - $z$  position. In DPHT, after transiting the periodic boundary, the particles are reset to the inlet temperature and then pass through the heat exchanger again. This “recycling” of particles is a strategy to keep the number of particles simulated to a minimum.

With the boundary temperatures, mass flow rate, and all particle properties aligned between the experiment and the simulation, the DEM and DPHT models were run. The key metric for comparison is the increase in mean temperature from the inlet to measurement location at 0.645 m from the inlet. The mean temperatures from the experiment and from the DPHT simulation are shown in Figure 11. DPHT predicts a mean temperature rise of 547 °C, compared to the experimentally found 570 °C, a difference of 4%. The details of the simulation and a discussion of the results follow.

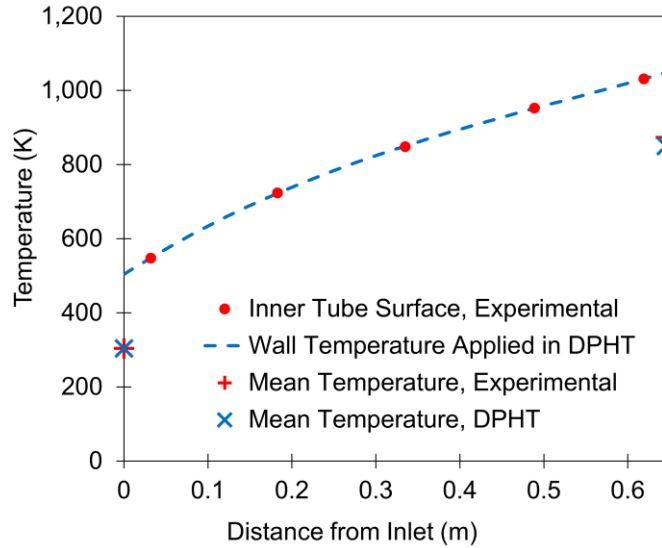


Figure 11. Inner wall temperature from experiment, and as applied as a boundary condition in DPHT with Eq. (30), along with the mean temperatures from the Watkins experiment (2018) and as calculated with DPHT.

The DEM simulation was run to find the positions of the particles over time, with a total of 135 seconds simulated. This required roughly four weeks of computation time, using 50 processors on a HPZ 840 Workstation with a clock speed of 2.8 GHz. The center coordinates of all particles were output every 2000 DEM time steps. The high computational cost shows this type of DEM simulation is limited to several million particles for feasible run times. For designing or optimizing heat exchangers, it is likely more reasonable to study a smaller, representative portion of a device.

The DPHT simulation was then run, which sequentially reads each particle position file output by DEM. Since heat transfer is only calculated at every 2000<sup>th</sup> DEM time step, the DPHT run was much shorter, finishing in several days. With 2000 DEM time steps per DPHT time step, the thermal time step size is 0.01 s. In reality, the duration of PP and PW collisions can be much faster than this, so using such a large DEM time step size implies some averaging of heat transfer rates across multiple collisions. This averaging is balanced out over many particle pairs and time steps, and the averaging does not make a difference in the final results as long as a sufficiently small DPHT time step is used. To verify this is the case, the time step was doubled to 0.02 s to verify that this did not change the overall results. Indeed, the total PW heat transfer was found to

be essentially identical for the two simulations, both in the initial transient time period and after reaching a steady state. Therefore it is concluded that 0.01 s is a sufficiently small time step. Note that the DEM simulation does not have to be rerun to check the effect of a larger thermal time step; only DPHT has to be rerun, with a larger thermal time step specified.

The steady state particle temperatures are shown in Figure 12. Image (a) shows a cross section of the particles, and the image has been compressed in the vertical direction to make it possible to visualize the long, thin tube. Moving from the inlet downward, the bulk temperature increases and a thermal boundary layer develops along the tube. The radial temperature profile at the outlet is shown in Figure 12(b). The temperature gradient is relatively severe, with a temperature difference between the inner- and outermost particles of 350 °C over a distance of only 5.41 mm. The shape of the curve is qualitatively similar to those by Watkins (2018). This high temperature gradient is due to the relatively poor thermal conductivity of the particle-fluid mixture and the low degree of mixing in dense granular flows. Mixing the flow to reduce this temperature gradient and increase heat transfer is the subject of Section 6.

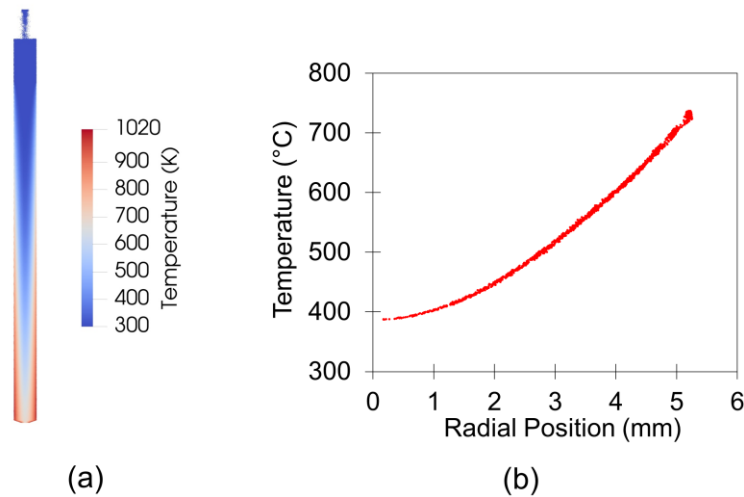


Figure 12. Steady state particle temperatures, showing (a) a cross-section of the tube (compressed in the vertical direction), and (b) the radial temperature profile at the outlet.

The heat flux at axial positions along the tube is shown in Figure 13, with each PW heat transfer mode shown separately. As is typical in simulations under these conditions, the PFW conduction

component is dominant. Heat transfer is highest near the inlet, where the temperature difference between the particles and the wall is the largest. Moving down the tube, a boundary layer forms, reducing the heat flux. Simultaneously, PFW conduction is enhanced due to the higher thermal conductivity of air at high temperatures, which may cause the slight increase in PFW heat flux between 0.1 and 0.3 m. The radiation component begins to climb as the temperatures increase along the tube length, as radiative transfer scales with the difference in each temperature to the fourth power. PP conduction is largely not affected by the temperature, and it remains relatively constant along the tube length. Overall, 85.6% of the PW heat transfer is through PFW conduction, 8.5% is through PW conduction, and 5.9% is through PW radiation. At a distance of 0.645 m from inlet, the proportion of heat fluxes is 82.5% (PFW conduction), 7.2% (PW conduction), and 10.3% (PW radiation). Though radiation contributes the least overall, this is in part due to the experimental conditions, with the inlet temperature of 30 °C. In a real CSP system, the particles are anticipated to cycle at high temperature (in the range of 500 to 1000 °C), so radiation is expected to be even more prominent at these temperatures. One shortcoming of using this data set for validation is that any error in the radiation or conduction models is not discernable, due to the dominance of the PFW heat transfer mechanism. A more thorough validation would start with a higher inlet temperature, so the relative magnitudes of the PW radiation and PFW conduction modes would be similar, allowing a better validation of the radiative modes.

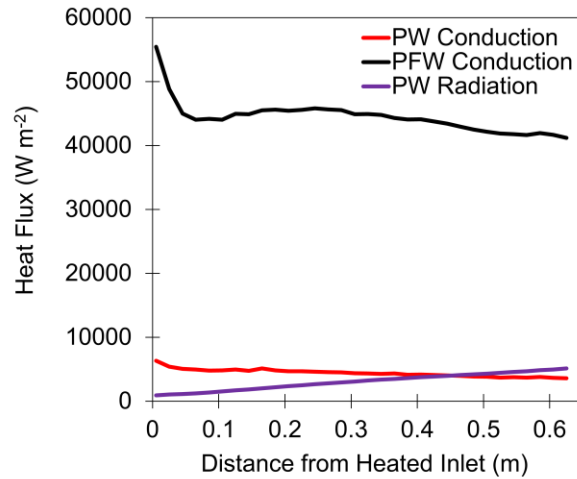


Figure 13. Particle-wall heat flux along the length of the tube, showing each particle-wall heat transfer mode.

The DEM properties for sintered bauxite are used because no values are available for zirconia-silica in literature, which may cause some discrepancy between the experiment and the simulation. The PP and PW friction coefficients used in the sliding and ‘rolling’ friction models are especially important for the characteristics of the flow to be realistic. If the PW frictional parameters are set too strong, they will slow down the flow along the tube surface, leading to a velocity profile, and heat transfer analysis, that is incorrect. This underscores the importance of DEM calibration before moving on to heat transfer modeling. A detailed calibration was performed for sintered bauxite particles by Grobbel (2019), which should give a reasonable approximation to the properties zirconia-silica particles.

The simulation shown here is one important step towards validating the DEM+DPHT model and other DEM-based heat transfer codes which use the same sub-models. The close match in overall heat transfer is a promising result, however, numerous experimental validation studies covering a range of conditions must be completed before these modeling methods can be trusted for highly accurate results. Ideally, such studies should cover various flow regimes and geometries commonly found in particle heat exchangers and solar receivers.



## 6. Heat Exchanger Design with DPHT

The configuration analyzed in the previous section is a good baseline case to study, but in a real heat exchanger or solar receiver, the performance can likely be improved by inducing mixing in the flow. If some geometry could be introduced to break up the thermal boundary layer, exchanging particles between the center and the wall, the PW heat transfer would increase. Continuum models for heat transfer in dense granular flow, such as the two-layer model by Watkins (2018) and the flat plate heat exchanger by Albrecht and Ho (2019), do not compute the details of particle collisions and mixing, so only the very simplest cases consisting of downward flowing particle streams without mixing can be analyzed. This shows the utility of the DEM-based approach, where different mixing geometries can be analyzed and evaluated.

As an initial analysis and a demonstration of the DPHT capabilities, a heat exchanger is analyzed, and two different methods for mixing are investigated. In the configuration studied, particles enter the top of the tube at 800 °C, and the tube wall has a temperature of 500 °C. In the base case, the heat exchanger is simply a heated tube in dense granular flow, with an orifice at the outlet (Figure 14). Next, a single horizontal plate is introduced, with an opening on one side to let the particles pass. Finally, a more complex “radial” mixer is studied. The radial mixer is designed to simultaneously transport particles on the interior directly towards the tube wall (through the four tubes) and to guide particles near the tube wall towards the center (via the funnel shape).

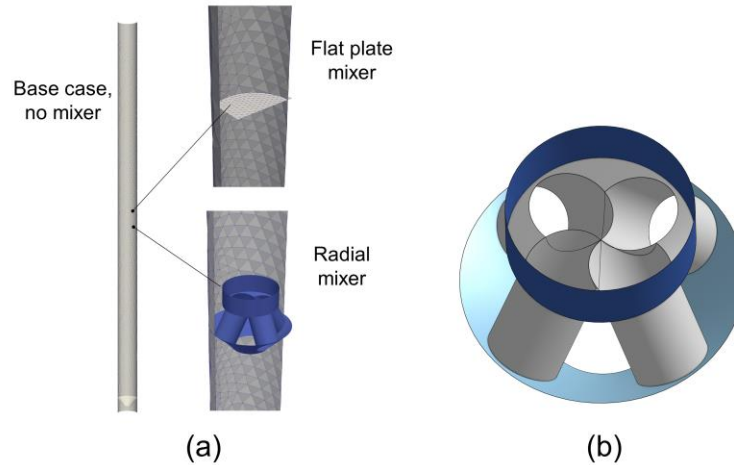


Figure 14. The heat exchanger analyzed, showing the (a) cross sections of base case and two potential improvements: a flat plate and a “radial” mixer, and (b) a close-up of the radial mixer.

In the DEM and DPHT simulations, the particle diameter is  $371.2\ \mu\text{m}$  to match the Sauter mean diameter of Carbo HSP 40/70 sintered bauxite particles (Johnson, 2021a), the DEM particle properties used are those of Carbo HSP 30/60 (Grobbel, 2019), and the tube diameter is 9 mm. The length of the tube is 18 cm, but the  $500\ \text{°C}$  boundary condition is only applied below 14.5 cm (measured from the outlet), above which the adiabatic boundary condition is specified. The simulations were run until the PW heat transfer was constant in time, meaning a steady state was reached. The steady state particle temperatures are shown in Figure 15 for the three cases. For the base case (Figure 15(a)), a high temperature gradient develops near the outlet, similar to the simulations in Section 4. In Figure 15(b), the flat plate shows relatively ineffective mixing, since the boundary layer appears almost undisturbed downstream of the plate. There is also a vacant gap where no particles touch the surface, representing a lost opportunity for heat transfer. The radial mixer (Figure 15(c)) greatly reduces the thermal gradients, and the close-up view shows how the near-wall and interior particles effectively switch places. With such effective mixing, a higher heat transfer is anticipated.

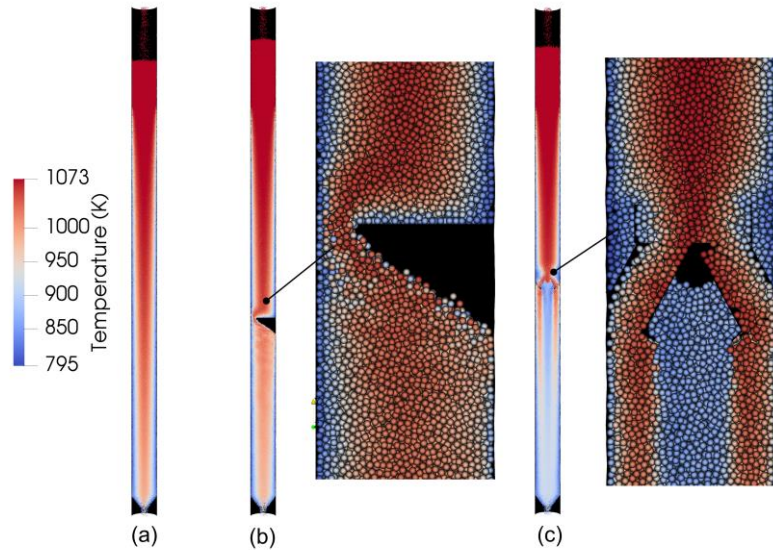


Figure 15. Cross section of the steady state particle temperatures for (a) base case, (b) flat plate, and (c) radial mixer.

The steady state heat flux along the tube length is shown in Figure 16 for the three cases. As expected, all show a high heat transfer rate near the entrance, which diminishes in the direction of flow. The flat plate mixer (green line) shows a drop in the heat flux at 0.07 m due to the vacant pocket below the plate. The plate must induce a slight amount of mixing, as the heat flux increases slightly at 0.09 m, but this gain just offsets the penalty caused by the pocket. Finally, the radial mixer (red line) also shows a drop in heat flux, since it also causes a small vacant pocket. However, the mixing benefit is much larger, and the heat flux stays higher until near the outlet. In terms of total heat transfer, the flat plate mixer has essentially the same heat transfer as that of the base case, whereas the radial mixer results in an enhancement of 8%. The radial mixer shows a much higher heat flux over the base case just downstream of the mixer, indicating that an increase of much more than 8% is possible by introducing multiple radial mixers.

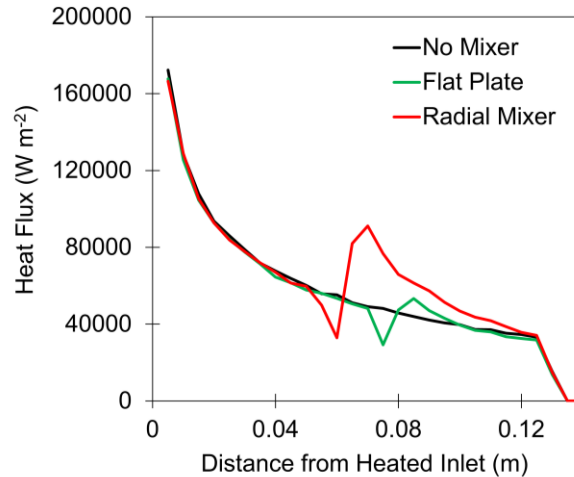


Figure 16. Particle-wall heat flux along the length of the tube, showing the three cases studied.

The mixing geometries studied here show that a significant improvement in heat transfer can be achieved over a non-mixed heated tube, and many envisioned designs can be analyzed with DPHT. Competing designs can be compared side-by-side, and results can be compared in terms of their heat transfer. As noted in Section 5, though early indications point to the accuracy of DPHT, DEM-based heat transfer modeling needs more experimental validation before it can be widely trusted for accurate quantitative results. However, before extensive validation has been done, similar heat exchanger designs can still be evaluated to gauge their relative effectiveness, as shown in this example.

Each of the simulations contained roughly 220,000 particles and took around 20 hours of computation time, most of which was spent on DEM. This shows that heat exchangers of small size can be analyzed and compared in an acceptable time period, but full-sized heat exchangers likely need some simplification. This may be done by dividing along planes of symmetry, if possible. Furthermore, if a heat exchanger consists of repeated sections (such as many parallel tubes), the computationally expensive DEM simulation can be run just once, and DPHT can be rerun with different temperature boundary conditions for the different sections.

In addition to mixing, the design can be modified in many ways to increase heat transfer, such as adding fins, reducing the tube diameter, increasing the wall and particle emissivities, or even

replacing air with a different interstitial gas. With DPHT provided as an open source code, others can now use it for studying and enhancing a variety of solid particle heat exchangers.

## 7. Conclusions

Dense granular flows are found in many solid particle CSP devices, yet the options for simulating heat transfer in these flows with DEM-based models have been limited. This manuscript introduces DPHT, which includes all of the relevant modes of particle-particle and particle-wall heat transfer. It is written in Julia, which is similar enough to interpreted languages (e.g. Matlab) that many researchers can understand and modify it. Although the heat transfer sub-models are based on published models, numerous modifications were made to make them more physically realistic.

As a test of the accuracy of DPHT, the experimental setup of a solar receiver by Watkins (2018) was modeled. The setup consisted of a dense granular flow of zirconia-silica particles through a heated tube, with the key metric being the increase in the mean temperature from inlet to outlet. The rise in mean temperature predicted by DPHT was 547 °C, compared to the experimentally measured 570 °C. The agreement to within 4% is promising, but more comparisons need to be done to further validate DPHT under a wider range of conditions.

To compare the particle-particle radiation models directly, a simulation was set up where radiation was the only mode of heat transfer. The DPHT and two “environment temperature” models from literature were each tested, and the results are compared to those of a highly accurate Monte Carlo simulation. DPHT showed a close agreement to the Monte Carlo simulation, whereas both of the environment temperature models showed a violation of the conservation of energy.

As an analysis to improve the effectiveness of tubular heat exchangers, a flat plate and a more complex “radial” mixer were introduced into the particle stream. Results indicate that a simple obstruction such as a flat plate tends to induce almost no mixing or enhancement in heat transfer. In contrast, the radial mixer resulted in an 8% increase in heat transfer overall, though a higher increase is likely possible by adding multiple mixers to keep the flow mixing throughout the heat

exchanger. With DPHT, many different designs can be analyzed and tested under identical boundary conditions to show which designs are most effective. In addition, being able to simulate and visualize particle temperatures and heat fluxes provides valuable intuition to researchers designing heat exchangers. The flow behavior and mixing of particles in these simulations must be done with DEM-based simulations, as continuum models cannot accurately model the friction and momentum transfer at the particle scale.

The goal of developing DPHT is to provide a solution for DEM-based heat transfer modeling of dense granular flows. It is well-documented and developed to the point where others can readily use it for the types of analyses shown in this work. It is published as an open source code so that others can download, use, and improve upon it. Researchers modifying DPHT are encouraged to publish their codes in an open source manner as well.

## **Acknowledgements**

We gratefully acknowledge Megan Kirschmeier (formerly Megan Watkins) for providing detailed data and information about the experimental setup in Section 4.

## **Funding Sources**

This research did not receive any specific grant from funding agencies in the public, commercial, or not-for-profit sectors.

## **References**

- Albrecht, K.J., Ho, C.K., 2019. Heat Transfer Models of Moving Packed-Bed Particle-to-sCO<sub>2</sub> Heat Exchangers. *J. Sol. Energy Eng.* 141, 1–8. <https://doi.org/10.1115/1.4041546>
- Bartsch, P., Baumann, T., Zunft, S., 2016. Granular Flow Field in Moving Bed Heat Exchangers: A Continuous Model Approach. *Energy Procedia* 99, 72–79. <https://doi.org/10.1016/j.egypro.2016.10.099>

- Batchelor, G.K., O'Brien, R.W., 1977. Thermal or Electrical Conduction Through a Granular Material. *Proc R Soc London Ser A* 355, 313–333. <https://doi.org/10.1098/rspa.1977.0100>
- Baumann, T., Zunft, S., 2015. Development and Performance Assessment of a Moving Bed Heat Exchanger for Solar Central Receiver Power Plants, in: *Energy Procedia*. Elsevier, pp. 748–757. <https://doi.org/10.1016/j.egypro.2015.03.085>
- Bezanson, J., Edelman, A., Karpinski, S., Shah, V.B., 2017. Julia: A fresh approach to numerical computing. *SIAM Rev.* 59, 65–98. <https://doi.org/10.1137/141000671>
- Bouvard, D., Argento, C., 1996. A ray tracing method for evaluating the radiative heat transfer in porous media. *Int. J. Heat Mass Transf.* 39, 3175–3180.
- Brennen, C., 2002. *Fundamentals of Multiphase Flow*. Cambridge University Press.
- Chaudhuri, B., Muzzio, F.J., Tomassone, M.S., 2010. Experimentally validated computations of heat transfer in granular materials in rotary calciners. *Powder Technol.* 198, 6–15. <https://doi.org/10.1016/j.powtec.2009.09.024>
- Chaudhuri, B., Muzzio, F.J., Tomassone, M.S., 2006. Modeling of heat transfer in granular flow in rotating vessels. *Chem. Eng. Sci.* 61, 6348–6360. <https://doi.org/10.1016/j.ces.2006.05.034>
- Cheng, G.J., Yu, A.B., Zulli, P., 1999. Evaluation of effective thermal conductivity from the structure of a packed bed. *Chem. Eng. Sci.* 54, 4199–4209. [https://doi.org/10.1016/S0009-2509\(99\)00125-6](https://doi.org/10.1016/S0009-2509(99)00125-6)
- Goniva, C., Kloss, C., Hager, A., Pirker, S., 2010. An open source CFD-DEM perspective. *Proc. OpenFOAM Work.* 1–10.
- Grobbel, J., 2019. *Modeling Solar Particle Receivers with the Discrete Element Method*. RWTH Aachen University.
- Gusarov, A. V., 2020. Radiative transfer, absorption, and reflection by metal powder beds in laser powder-bed processing. *J. Quant. Spectrosc. Radiat. Transf.* 257. <https://doi.org/10.1016/j.jqsrt.2020.107366>
- Hicdurmaz, S., Johnson, E., Grobbel, J., Amsbeck, L., Buck, R., Hoffschmidt, B., 2020. Numerical Heat Transfer Modelling of a Centrifugal Solar Particle Receiver, in: *AIP Conference Proceedings (Currently under Review)*.
- Hicdurmaz, S., Tari, I., 2018. Numerical Investigaton of Bubbling Fluidized Bed to be Used as Thermal Energy Storage Integrated to High-Temperature Concentrated Solar Power. *Multiph. Sci. Technol.* 30, 1–22. <https://doi.org/10.1615/MultScienTechn.2018024729>
- Johnson, E., Baker, D., Tari, I., 2017. Proposal of a Novel Gravity-Fed , Particle-Filled Solar Receiver, in: *AIP Conference Proceedings*. American Institute of Physics. <https://doi.org/10.1063/1.4984371>
- Johnson, E., Tari, I., Baker, D., 2020. A Monte Carlo method to solve for radiative effective

- thermal conductivity for particle beds of various solid fractions and emissivities. *J. Quant. Spectrosc. Radiat. Transf.* 250. <https://doi.org/10.1016/j.jqsrt.2020.107014>
- Johnson, E.F., 2021a. *Advances in Modeling High Temperature Particle Flows in the Field of Concentrating Solar Power*. Middle East Technical University, <https://open.metu.edu.tr/handle/11511/89717>.
- Johnson, E.F., 2021b. GitHub - ef-johnson/Dense-Particle-Heat-Transfer [WWW Document]. GitHub. URL <https://github.com/ef-johnson/Dense-Particle-Heat-Transfer> (accessed 4.9.21).
- Johnson, E.F., 2021c. GitHub - ef-johnson/Ray-Tracing-Many-Spheres [WWW Document]. GitHub. URL <https://github.com/ef-johnson/Ray-Tracing-Many-Spheres> (accessed 4.9.21).
- Johnson, E.F., Tari, İ., Baker, D., 2021. Radiative heat transfer in the discrete element method using distance based approximations. *Powder Technol.* 380, 164–182. <https://doi.org/10.1016/j.powtec.2020.11.050>
- Julia Micro-Benchmarks [WWW Document], 2020. URL <https://julialang.org/benchmarks/> (accessed 11.29.20).
- Kloss, C., Goniva, C., Hager, A., Amberger, S., Pirker, S., 2012. Models , algorithms and validation for opensource DEM and CFD-DEM. *Prog. Comput. Fluid Dyn.* 12, 140–152. <https://doi.org/10.1504/PCFD.2012.047457>
- Komossa, H., Wirtz, S., Scherer, V., Herz, F., Specht, E., 2015. Heat transfer in indirect heated rotary drums filled with monodisperse spheres: Comparison of experiments with DEM simulations. *Powder Technol.* 286, 722–731. <https://doi.org/10.1016/j.powtec.2015.07.022>
- Krause, B., Liedmann, B., Wiese, J., Bucher, P., Wirtz, S., Piringer, H., Scherer, V., 2017. 3D-DEM-CFD simulation of heat and mass transfer, gas combustion and calcination in an intermittent operating lime shaft kiln. *Int. J. Therm. Sci.* 117, 121–135. <https://doi.org/10.1016/j.ijthermalsci.2017.03.017>
- MFS Development Group, 2021. *MFIX User Guide, Release 21.1*.
- Morris, A.B., Ma, Z., Pannala, S., Hrenya, C.M., 2016. Simulations of heat transfer to solid particles flowing through an array of heated tubes. *Sol. Energy* 130, 101–115. <https://doi.org/10.1016/j.solener.2016.01.033>
- Musser, J.M.H., 2011. *Modeling of heat transfer and reactive chemistry for particles in gas-solid flow utilizing continuum-discrete methodology (CDM)*. PhD Thesis West Virginia University.
- Niederwestberg, S., Schneider, F., Boura, C., Herrmann, U., 2020. Introduction to a Direct Irradiated Transparent Tube Particle Receiver, in: *AIP Conference Proceedings (Currently under Review)*.
- Norouzi, H.R., Zarghami, R., Sotudeh-gharebagh, R., Mostoufi, N., 2016. *Coupled CFD - DEM Modeling*, 1st ed. John Wiley & Sons.



- Oschmann, T., Schiemann, M., Kruggel-Emden, H., 2016. Development and verification of a resolved 3D inner particle heat transfer model for the Discrete Element Method (DEM). *Powder Technol.* 291, 392–407. <https://doi.org/10.1016/j.powtec.2015.12.008>
- Qi, F., Wright, M.M., 2018. Particle scale modeling of heat transfer in granular flows in a double screw reactor. *Powder Technol.* 335, 18–34. <https://doi.org/10.1016/j.powtec.2018.04.068>
- Ruiz, G., Ripoll, N., Fedorova, N., Zbogar-Rasic, A., Jovicic, V., Delgado, A., Toledo, M., 2019. Experimental and numerical analysis of the heat transfer in a packed bed exposed to the high thermal radiation flux. *Int. J. Heat Mass Transf.* 136, 383–392. <https://doi.org/10.1016/j.ijheatmasstransfer.2019.03.009>
- Siegel, N.P., Gross, M.D., Coury, R., 2018. The Development of Direct Absorption and Storage Media for Falling Particle Solar Central Receivers 137, 1–7. <https://doi.org/10.1115/1.4030069>
- Syamlal, M., Rogers, W., Thomas, O., 1993. MFIx Documentation Theory Guide.
- Tien, C.L., 1988. Thermal Radiation in Packed and Fluidized Beds. *J. Heat Transfer* 110, 1230. <https://doi.org/10.1115/1.3250623>
- Watkins, M.F., 2018. A Heat Transfer Analysis of Vertical Dense Granular Flows. North Carolina State University.
- Yang, R.Y., Zou, R.P., Yu, A.B., 2002. Voronoi tessellation of the packing of fine uniform spheres. *Phys. Rev. E - Stat. Physics, Plasmas, Fluids, Relat. Interdiscip. Top.* 65, 8. <https://doi.org/10.1103/PhysRevE.65.041302>
- Zhou, Z.Y., Yu, A.B., Zulli, P., 2010. A new computational method for studying heat transfer in fluid bed reactors. *Powder Technol.* 197, 102–110. <https://doi.org/10.1016/j.powtec.2009.09.002>
- Zhou, Z.Y., Yu, A.B., Zulli, P., 2009. Particle Scale Study of Heat Transfer in Packed and Bubbling Fluidized Beds. *AIChE J.* 55, 868–884. <https://doi.org/10.1002/aic>

Definition of Open Access Pathways Allowed by the  
Publisher that are Used to Publish this Manuscript Open Access

## Sherpa Romeo

## Solar Energy

## Publication Information

Title	Solar Energy [English]
ISSNs	Print: 0038-092X
URL	<a href="http://www.elsevier.com/wps/product/cws_home/329/description">http://www.elsevier.com/wps/product/cws_home/329/description</a>
Publishers	Elsevier [Commercial Publisher] International Solar Energy Society [Associate Organisation]






## Publisher Policy






Open Access pathways permitted by this journal's policy are listed below by article version. Click on a pathway for a more detailed view.

Published Version [pathway a]	   None  CC BY-NC-ND 	 PMC, Non-Commercial Repository, Research for Development Repository, +2 <span style="float: right;">+</span>
----------------------------------	--	--





Published Version [pathway b]	   None  CC BY 	 Institutional Repository, Subject Repository, PMC, Research for Development Repository, +2 <span style="float: right;">+</span>
----------------------------------	--	---

Published Version [pathway c]	   None  CC BY  PMC 	 Institutional Repository, Subject Repository, PMC, Research for Development Repository, +2 <span style="float: right;">+</span>
----------------------------------	--	---

Accepted Version [pathway a]	 None  CC BY-NC-ND  	 arXiv, RePEc, Author's Homepage <span style="float: right;">-</span>
---------------------------------	--	--

 Embargo	No Embargo
 Licence	CC BY-NC-ND
 Location	Author's Homepage Named Repository (arXiv, RePEc)
 Conditions	Must link to publisher version with DOI
 Notes	Authors can share their accepted manuscript immediately by updating a preprint in arXiv or RePEc with the accepted manuscript

Accepted Version [pathway b]	 24m  CC BY-NC-ND 	 Institutional Repository, Subject Repository <span style="float: right;">-</span>
---------------------------------	---	---

 Embargo	24 Months
 Licence	CC BY-NC-ND
 Location	Institutional Repository Subject Repository
 Conditions	Must link to publisher version with DOI

Accepted Version [pathway c]	  12m  CC BY-NC-ND 	 Institutional Repository, Subject Repository <span style="float: right;">+</span>
---------------------------------	---	---

Submitted Version	 None  Any Website, +2 <span style="float: right;">+</span>
-------------------	---

For more information, please see the following links:

- [Sharing Policy](#)
- [Green open access](#)
- [Unleashing the power of academic sharing](#)
- [Journal Embargo List for UK Authors](#)
- [Open access](#)
- [Funding Body Agreements](#)
- [Attaching a User License](#)
- [Sharing and Hosting Policy FAQ](#)
- [Open access licenses](#)
- [Article Sharing](#)
- [Journal Embargo Period List](#)

## Record Information

Sherpa Romeo information is accurate to the best of our knowledge but should not be relied upon for legal advice.

[Suggest an update for this record](#)

Useful links

- [Open access services from Jisc](#)
- [Guide to managing open access costs](#)
- [Open access guides by Jisc](#)

Contact

[help@jisc.ac.uk](mailto:help@jisc.ac.uk)

Accessibility

[Accessibility Statement](#)



Digital resources

- [Maps and spatial data](#)
- [Library support](#)

- [Learning and research resources](#)
- [Open access \(OA\)](#)

We provide secure, cost-effective access to the UK's richest collection of digital content: giving you access to the latest data and content from leading international publishers and providers.

[Find out more at jisc.ac.uk](http://jisc.ac.uk)



This work is licensed under the [CC BY-NC-ND 4.0](#)  
[About using our content](#)